*Science & Technology Development Journal, 23(3):602-609*

Open Access Full Text Article

*Research Article*

# $SrTiO_3$ nanocubes doped with ir as photocatalytic system for enhancing $H_2$ generation from water splitting

**Ton Nu Quynh Trang[1], Tieu Tu Doanh[1,2], Do Thanh Sinh[2], Vu Thi Hanh Thu[1,*]**

Use your smartphone to scan this QR code and download this article

**ABSTRACT**

**Introduction**: Designing an effective photocatalyst for hydrogen ($H_2$) performance under visible irradiation with a decrease the bandgap energy of semiconductor has been considered as an essential aspect in boosting the performance of photocatalytic reactions for hydrogen performance from the water-splitting process. Herein, we focus on evaluating the role of doping with Ir into $SrTiO_3$ structure fabricated by the hydrothermal method for $H_2$ generation. **Methods**: The crystalline characteristics of the Ir-$SrTiO_3$ photocatalyst were carried out via X-ray powder diffraction (XRD) and field emission scanning electron microscopy (FE-SEM). The chemical composition and the optical properties of the Ir-$SrTiO_3$ were classified by energy-dispersive X-ray spectroscopy (EDX) and UV-Vis spectra, respectively. **Results**: The results showcased that the dramatically improved absorbing performances of Ir/$SrTiO_3$ specimen were observed. This could be governed by the presence of Ir impurity states in the forbidden energy gap, causing a decrease in the energy gap of $SrTiO_3$. This work also revealed that Ir doped into $SrTiO_3$ nanocube structure exhibited excellent photocatalytic $H_2$ evolution compared with pristine $SrTiO_3$ (~454 and ~325 mmol.$h^{-1}$.$g^{-1}$ $H_2$ production under UV and visible light irradiation, respectively). A rational photocatalytic mechanism is projected to be able to provide significant awareness for further research. **Conclusion**: The results are believed to be the role of Ir states and nanocube structures of $SrTiO_3$ as a new approach in renewable energy resources.

**Key words:** SrTiO3, water splitting, visible light, transition metal

## INTRODUCTION

Nowadays, the rapid depletion and combustion of fossil fuels and global warming effects have become challenges increasingly. To tackle the issues of environmental crisis and usage of sustainable sources, as well as renewable technologies, have attracted the widespread concerns in recent years [1–3]. As a promising hydrogen ($H_2$) energy, the hydrogen evolution reaction (HER) from water by photocatalytic water splitting has been widely used as a renewable energy source to solve the global challenges concerning the crisis of energy and the environment. In this regard, semiconductor photocatalysis applied for $H_2$ evolution has been developed widely because of its outstanding contributions in environmental treatment systems [4–6]. This approach bases on the formation of photogenerated electron-holes pairs from the semiconductor catalyst under suitable light irradiation. The generation of photoexcited charge carriers is changed into reactive oxygen species (ROS) to split the water to $H_2$ gas formation [7–9]. Among these semiconductors developed in the recent year, titanium dioxide ($SrTiO_3$) has been widely used in this field due to its non-toxic, cheap, environment-friendly, stable against corrosion and photo-corrosion and the rapid the photoinduced electron-hole pairs under light excitation, contributing enhanced photocatalytic behaviors [10,11]. Nevertheless, it's photocatalytic efficient has still hindrance related to two main drawbacks: i) $SrTiO_3$ has a large forbidden energy gap ($E_g$ = 3.2 eV) and is thus only promote in the UV light irradiation, which has occupied for 3–5% of total solar spectrum [12]; ii) the rapid recombination rate of chare carriers has remained crucial challenges, leading to restricted the photocatalytic performance of $SrTiO_3$ [5,13]. To overcome these weaknesses, effective strategies to enhance photocatalytic performance has progressed at a fast pace. For example, Pt-loaded Rh-doped $SrTiO_3$ exhibited a remarkably high photoelectrochemical behavior and the conversion of alcohol to efficiently form $H_2$ under visible light. This result was attributed to the well-driven energy band structures of the semiconductor via Rh doping, which provided the appropriate oxidation capabilities of photogenerated holes [14]. In addition, co-doping with tantalum and chromium ($TiO_2$:Ta/Cr) or nickel and tantalum or niobium ($TiO_2$:Ni/(Ta, Nb) showed a high photocatalytic performance response under visible light due

[1]*Faculty of Physics and Engineering Physics, VNUHCM-University of Science*

[2]*Saigon Hitech Park Labs*

**Correspondence**

**Vu Thi Hanh Thu**, Faculty of Physics and Engineering Physics, VNUHCM-University of Science

Email: vththu@hcmus.edu.vn

**History**

- Received: 2020-05-31
- Accepted: 2020-08-18
- Published: 2020-08-24

**DOI : 10.32508/stdj.v23i3.2403**

Check for updates



VNU-HCM Press

**Cite this article :** Trang T N Q, Doanh T T, Sinh D T, Thu V T H. **$SrTiO_3$ nanocubes doped with ir as photocatalytic system for enhancing $H_2$ generation from water splitting** . *Sci. Tech. Dev. J.;* 23(3):602-609.

to the presence of the occupied d orbitals of metals that created electron donor levels and subbands in the bandgap of $TiO_2$ [15,16]. Therefore, it is acknowledged that doping transition metal into semiconductor plays a significant role in the enhanced photocatalytic activity for $H_2$ generation.

Among these approaches, transition metal ion doping into $SrTiO_3$ nanostructures has attracted enormous attention owing to several reasons i) increasing in the visible light absorption capacity of $SrTiO_3$ in the visible region due to the presence of impurities at different levels in the energy bandgap and the localized surface plasmon resonance (LSPR); ii) the fast recombination rate of photoinduced charge carriers hamper many charge transfer reactions; iii) the appearance of the Schottky barrier can be created at the interface, leading to decrease the charge recombination process. Among all kinds of transition metal co-photocatalyst, Iridium (Ir) has been considered as one of the most promising candidates on account of its ease of dispersion on some carriers and the high carrier mobility of electronic structures based on d orbital transition [17,18]. The recent studies exhibited that doping with cations into $SrTiO_3$ structures suppressing backward reactions has more effective for improving the photocatalytic performance of $SrTiO_3$ photocatalysts during water splitting process, attributing the presence of large active sites and the defect levels in forbidden corresponding to the interband transitions of metals and semiconductor. For example, doping with Rh, Ru, and Ir into $SrTiO_3$ structures showed high activity for hydrogen evolution under the visible irradiation. Koto et al. [19] reported that the pairs of Cr-Sb, Cr-Ta, and Ni-Ta codoped $SrTiO_3$ photocatalysts and evaluated the $H_2$ performance. The results have shown that doping with Cr-Ta showed higher photocatalytic behavior in comparison with only Ta doping. Ma et al. showcased that $H_2$ evolution rate from water based on transition metal doped $SrTiO_3$ structure was higher than that of bare $SrTiO_3$ [20]. Based on these phenomena, this work focuses on the Ir doped into $SrTiO_3$ structure by a hydrothermal treatment. The results indicate that the efficiency of photocatalyst for improving the hydrogen evolution under UV-vis-light irradiation is observed by the effective separation of photogenerated charges and the appearance of matching energy levels of the midgap states in the forbidden energy gap of the semiconductor.

# EXPERIMENT

## Materials

Titanium tetrachloride ($TiCl_4$, Aldrich Chemical, <99%), strontium nitrate ($Sr(NO_3)_2$, Sigma-Aldrich <99%), iridium (III) chloride hydrate ($Cl_3H_2IrO$, Sigma-Aldrich, <99%), hydrochloric acid (HCl, Merck, <37%), and methanol ($CH_3OH$, Merck, <99.9%). The chemical reagents were used without any further purification. Double distilled water using overall the experiments were obtained from Research Laboratories of Saigon Hi-Tech Park.

## Preparation of Ir-$SrTiO_3$ photocatalyst

Ir-$SrTiO_3$ nanoparticles have been successfully obtained using the hydrothermal method. The schematic for the preparation of Ir-$SrTiO_3$ is displayed in Figure 1. First, 20 mL of a 0.5 M $TiCl_4$ aqueous solution as the Ti precursor with 0.1 wt%. of $IrCl_3.xH_2O$ used as the metal Ir-precursor was added with 60 mL of DI and stirred for 30 min, denoted a mixture. Secondly, a proper amount of $Sr(NO_3)_2$ dissolved in 10 ml of 2M KOH solution was added to the reaction mixture. The solution was stirred for 30 minutes. The obtained suspension was then placed into an autoclave and kept at 200°C for 4 hours. The precipitates were experienced by the centrifugation process to gather the samples. After that, it was washed several times with double distilled water to eliminate the impurities. Finally, the specimen was dried under nitrogen gas flow.

## Characterization

X-ray powder diffraction (XRD, a Bruker D8 ADVANCE) with a Cu Ka source was used to determine the crystalline phase of the synthesized photocatalysts. The morphology of Ir-$SrTiO_3$ photocatalyst was acquired by the field emission scanning electron microscopy (FESEM, Hitachi S-4800). Its chemical components were investigated through energy-dispersive X-ray spectroscopy (EDX).

The photocatalytic behavior of $H_2$ performance of water-splitting of the as-prepared Ir-$SrTiO_3$ photocatalyst was performed using aqueous methanol. The samples as prepared photocatalyst were positioned at the bottom of 500 ml quartz cell with 200 ml $CH_3OH$ aqueous solution. The Pyrex glass reactor was directly exposed under UV lamp (wavelength from 320 nm to 400 nm) and visible lamp as the light source. The amount of generated gaseous product was determined hourly by an off-line gas chromatography equipped with a thermal conductivity detector (TCD).

# RESULTS

Characterization of the phase purity and crystallinity of the photocatalyst was thoroughly investigated by X-ray diffraction patterns. These results are displayed in

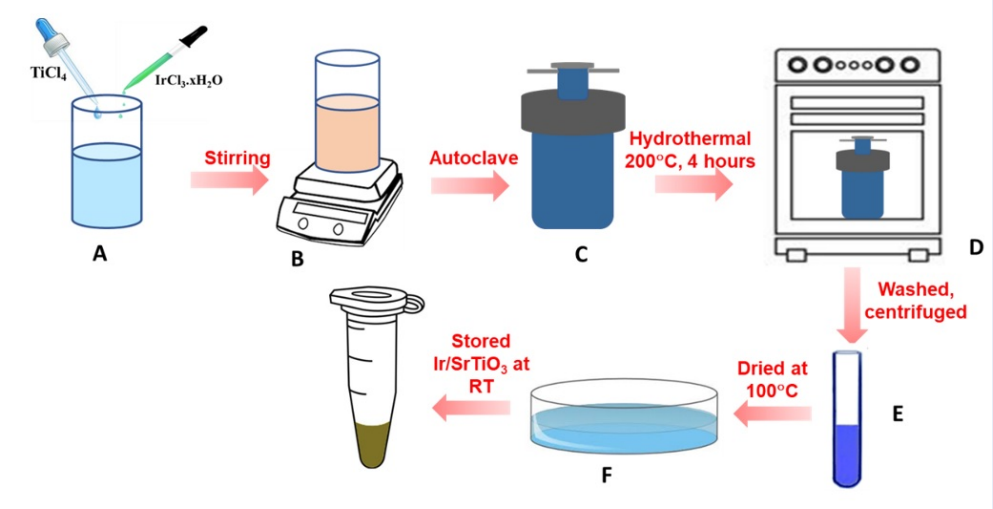


**Figure 1**: Schematic for the preparation of Ir doped $SrTiO_3$ photocatalyst: (A) Preparation of the precursors, (B) Stirring until the pH ofthe solution stabilizes, (C) The achieved suspension was transferred to anautoclave; (D) Fabricate of Ir doped $SrTiO_3$ through the hydrothermal method at 200 °C for 4 hours, (E) The centrifugation process to collect the sample and (F) The sample was dried under nitrogen gas flow.

Figure 2. The diffraction peaks appeared at 2q = 31°, 40°, 46°, 52.5°, 58°, 68°, and 77° which were corresponded to the diffraction of the (110), (111), (200), (210), (211), (220) and (310) crystal planes, respectively (JCPDS cards no. 74-1296) that was attributed to the cubic close-packed structure of $SrTiO_3$ (marked with *). Notably, no peak corresponding to impurity states such as $TiO_2$ and SrO have been observed in the spectrum. Nevertheless, Ir doped $SrTiO_3$ specimen did not show the characteristic peaks of Ir due to the low quantity; similar results would be found in the previous report[21]. As compared to $SrTiO_3$, Ir-$SrTiO_3$ photocatalyst exhibited a slight shift towards higher $2\theta$ scattering angles due to the replacement of $Ti^{4+}$ (0.605 Å) for $Ir^{3+}$ (0.625)[22,23].

The morphology properties of pristine $SrTiO_3$ and Ir-$SrTiO_3$ were characterized by FESEM images as shown in Figure 3. The results reveal that a large number of aggregated cuboid nanoparticles composed of very fine primary particles was small diameter (~50–80 nm) (Figure 2 a). Figure 2 b displays the SEM image of Ir-$SrTiO_3$ obtained by the doping process of Ir. The result shows that there was no significant change observed in surface morphology compared to the pristine $SrTiO_3$ after doping procedures. The results suggested that doping of Ir into $SrTiO_3$ structure did not significantly affect to the morphology of photocatalyst.

Furthermore, to further verify the existence of the elemental composition of the Ir-$SrTiO_3$, EDX spectra was achieved and shown in Figure 4. The result shows that the existence of Sr, Ti, O, and Ir were detected in the photocatalyst (Figure 4 (a-d)) with the EDX elemental map and The weight percentage of elements analyzed by EDX corresponding wt.% as shown in the table Figure 4 (e,f). The appearance of Ir species indicated that Ir species were successfully deposited onto $SrTiO_3$ structures. The peak intensity corresponding to the concentration level of the element in the $SrTiO_3$ was observed. Despite of low doping concentration of Ir, the peaks showed to be homogenously anchored in the photocatalyst structure.

The UV–vis absorbance spectra of pristine $SrTiO_3$ and Ir-$SrTiO_3$ photocatalysts were studied to reveal the optical properties of a sample. The characterization of absorption and the energy bandgap was determined by Kubelka-Munk equation, as depicted in Figure 5. It can be observed that the $SrTiO_3$ structures unveil a strong absorption edge (Figure 5 a) related to the large bandgap energy of 3.2 eV (Figure 5 b), which was assigned to the transfer of valence band to the conduction band. These results were consistent with previous works[24]. The absorption band of Ir doped into $SrTiO_3$ sample shows a significant shift to longer wavelengths at nearly 478 nm with respect to the bandgap of 2.1 eV (Figure 5 b), which can be assigned to some reasons: i) electron transition from the $Ir^{3+}$ occupied levels present above the valance band to the conduction band of $SrTiO_3$, causing the expansion of the absorption edge in the visible-light-driven; ii) the transition from Ir 3d electrons to the

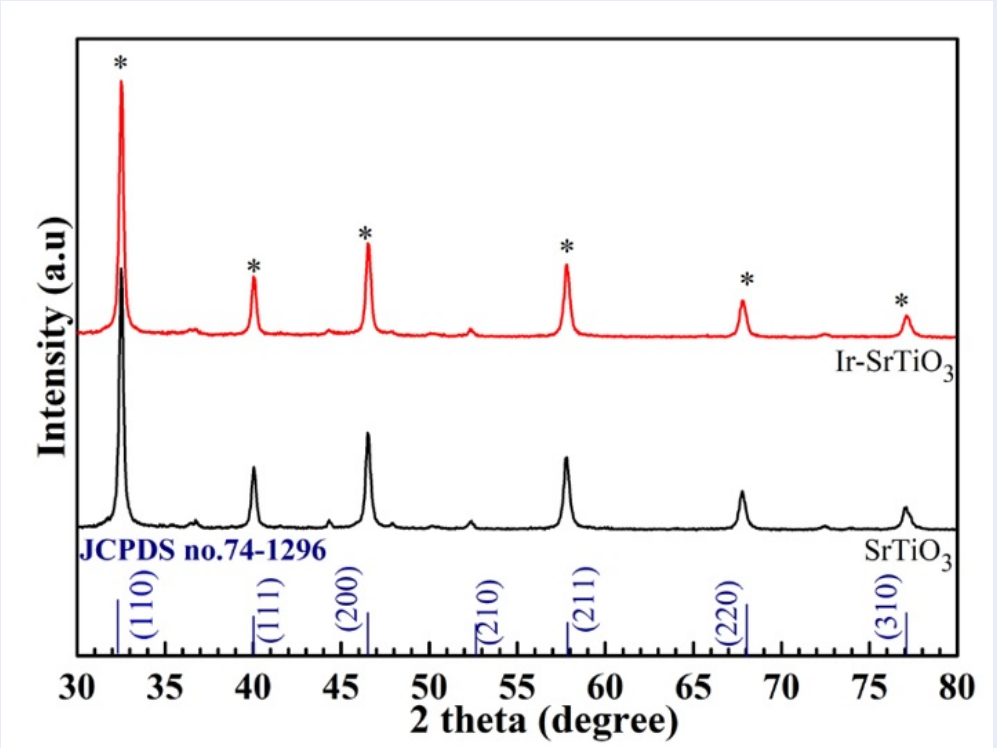


**Figure 2**: The crystalline characteristics through XRD patterns of as-prepared $SrTiO_3$ and Irdoped $SrTiO_3$ photocatalyst.

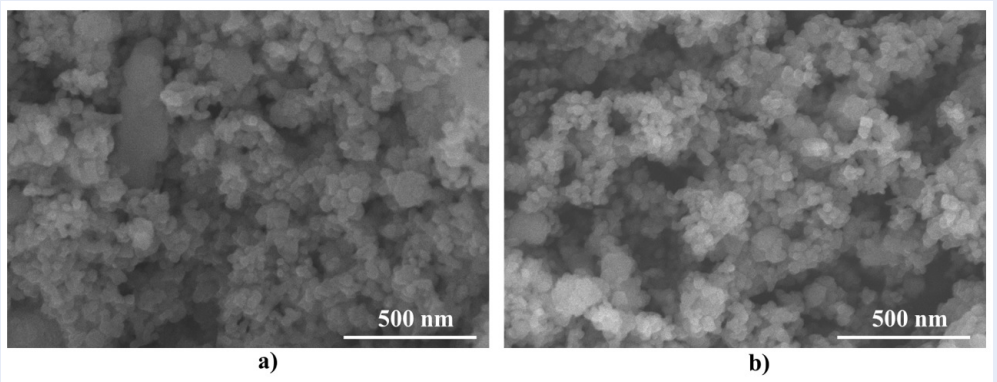


**Figure 3**: The morphological features of photocatalyst (a, b) SEM image of the pristine $SrTiO_3$, and Ir doped $SrTiO_3$ photocatalyst, respectively.

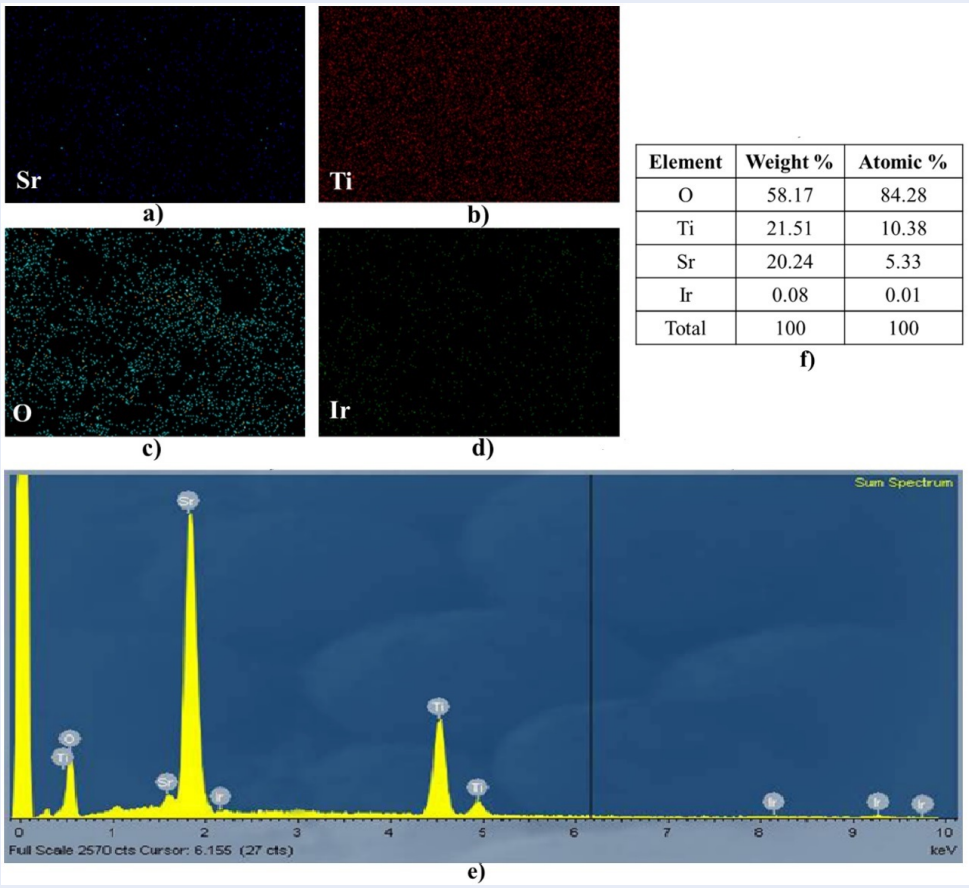


| Element | Weight % | Atomic % |
|---|---|---|
| O | 58.17 | 84.28 |
| Ti | 21.51 | 10.38 |
| Sr | 20.24 | 5.33 |
| Ir | 0.08 | 0.01 |
| Total | 100 | 100 |

f)

**Figure 4**: EDX elemental maps and an elemental component of the as-prepared Ir doped $SrTiO_3$ photocatalyst. (a, b, c, d) elemental mapping of Sr, Ti, O, and Ir, respectively, (e) EDX elemental map of Ir doped $SrTiO_3$, and (f)the composition percentage for all elements present in Ir doped $SrTiO_3$.

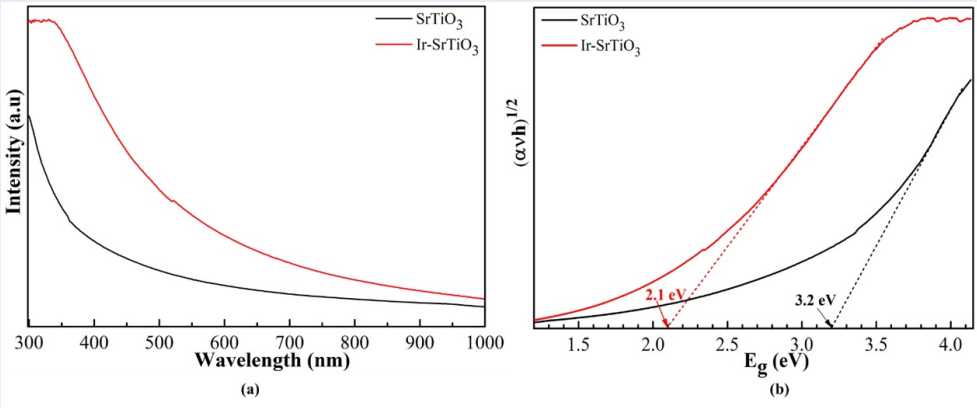


**Figure 5**: The absorption characteristics of the photocatalyst. (a) The UV–Vis absorption spectra and (b) plot of $(ahn)^{1/2}$ vs. photon energy of pristine $SrTiO_3$ andas-prepared Ir doped $SrTiO_3$.

conduction band of $SrTiO_3$. As a result, a narrower bandgap energy was obtained after doping with Ir into $SrTiO_3$. The results are similar to previously published data [25,26].

To assess the role of doping with Ir on photocatalytic $H_2$ evolution with $SrTiO_3$. The performance of photocatalytic $H_2$ production in the $SrTiO_3$ and Ir-$SrTiO_3$ was investigated using a $CH_3OH$ aqueous solution as a hole scavenger and direct exposure to UV and visible light, as presented in Figure 6. It can be clearly seen that the photocatalytic performances for hydrogen generation of Ir-$SrTiO_3$ exhibited a superior compared with that of pristine $SrTiO_3$ under both UV light and visible light. Especially, it can be found that Ir-$SrTiO_3$ photocatalyst possesses a dramatic $H_2$ evolution with the amount of ~325 $mmol.h^{-1}.g^{-1}$, which was more than 14-fold as much as that of $SrTiO_3$ under visible light, whereas, no $H_2$ production is detected under visible illumination. This could be assigned to the fact that the pristine $SrTiO_3$ photocatalyst is not activated under visible regime irradiation because of the large bandgap energy that is only driven by ultraviolet light, leading to low $H_2$ efficacy. On the other hand, doping Ir into $SrTiO_3$ structure, the photocatalyst would be activated under the visible light, thanks to the reduced forbidden energy gap related to the existence of impurity levels in the bandgap energy. As a result, the photoinduced charge carriers made the redox reactions to produce $H_2$ gas; thus, the photocatalytic $H_2$ generation would be significantly improved under the visible region illumination. The recycling stability of the photocatalyst is also an essential factor in evaluating its performance. Hence, the reusability of photocatalyst for $H_2$ evolution was performed through repeated cycles under visible light irradiation. As displayed in Figure 6, the $H_2$ production activities of Ir-$SrTiO_3$ stayed constant after four cycles, indicating the high stability of photocatalyst toward potential practices in renewable energy technologies.

## DISCUSSION

Based on a series of characterization, an appropriate reaction mechanism for photocatalytic $H_2$ generation regarding the generation of photoinduced charge carriers have been proposed. When the photocatalyst is activated by photon energy equal or greater than their forbidden energy gap, photogenerated electron–hole pairs are excited. These electrons undergo photocatalytic decomposition of water reduction and reduce $H^+$ to produce $H_2$ molecules. On the other hand, the photoinduced holes at the valance band react quickly with $H_2O$ to form hydroxyl radicals in a consecutive reaction route. Compared with the photocatalytic activity for $H_2$ generation of bare $SrTiO_3$, the $H_2$ production of Ir doped $SrTiO_3$ specimen enhanced significantly, which means that the doping with Ir could decrease the forbidden band of the semiconductor as shown in Figure 5 and prevent the rapid recombination process of photoinduced charge carriers, while most photogenerated charge carriers in pristine $SrTiO_3$ could be quickly recombined, resulting in low photocatalytic behavior. Moreover, doping with Ir into $SrTiO_3$ structure could appear some defects in the forbidden band as shown in the outcomes of UV-Vis section; these defects are believed to be the active sites in photocatalytic reaction contributing the enhancement of $H_2$ photocatalytic. In the whole process, a positive effect of charge carrier performance related to the defects providing effective separation of photogenerated **chare** carriers are obtained. There are no detailed studies for the water-splitting efficiency in Ir-$SrTiO_3$ samples. In recent research, a similar kind of trend was observed by Fadlallah et al. for cation codoped $SrTiO_3$ photocatalysts for water splitting. Photocatalytic activity of $SrTiO_3$ codoped metal transition such as Rh, V, Sb significantly improved as compared to pristine $SrTiO_3$ due to the reduction of the bandgap energy of host structure [27]. Ma et al. reported that the $H_2$ production from water splitting of transition metal-doped $SrTiO_3$ photocatalysts exhibited higher than that of pristine $SrTiO_3$ due to the presence of sub-bandgap states in the $SrTiO_3$ lattice under visible light [28]. Therefore, the results of our research showcase the high $H_2$ evolution at a wavelength of 590 nm (Ir doped $SrTiO_3$ specimen exhibited both UV light and visible light irradiation). These results from this research provide an insight into the role of the photocatalyst in potential practices for renewable energy technologies.

## CONCLUSION

In conclusion, Ir elements have successfully doped into the perovskite structure of $SrTiO_3$ by hydrothermal method. The phase content and structure characterization did not change dramatically after doing with Ir. Compared to those of pristine $SrTiO_3$, the improved absorption capability of Ir-$SrTiO_3$ specimen in the visible light was observed. Moreover, doping Ir into $SrTiO_3$ structure exhibited a dramatically improved visible-light-driven photocatalytic $H_2$ evolution performance. The $H_2$ evolution could reach up to ~325 $mmol.h^{-1}.g^{-1}$ under visible light irradiation after 180 minutes. This may be assigned to the productive charge separation of photogenerated electron-hole pairs and the reduction of the forbidden

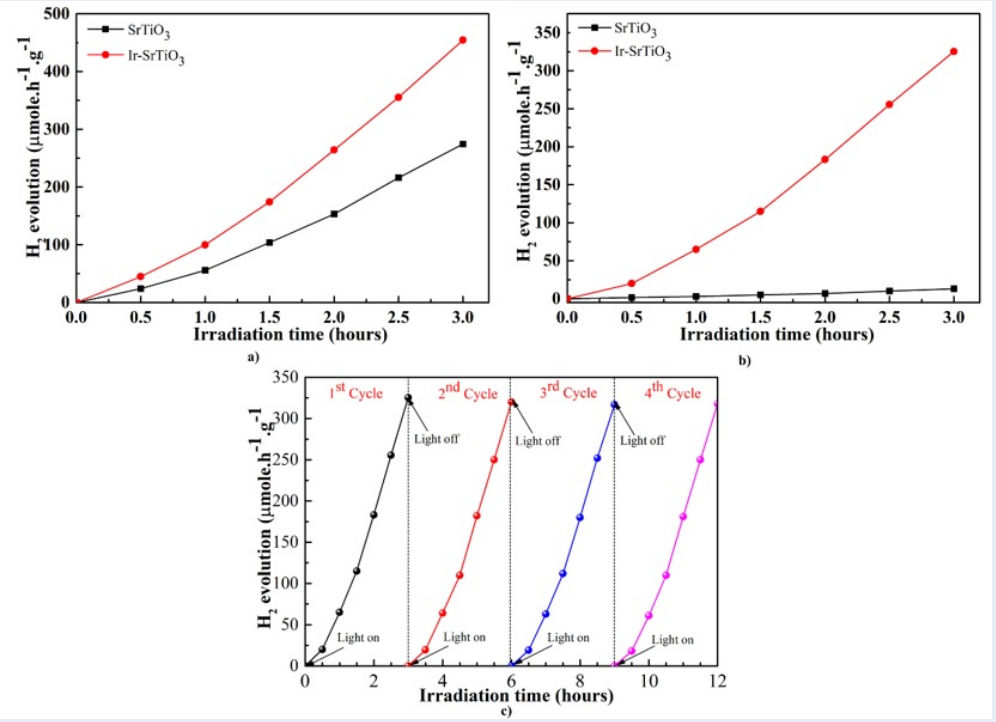


**Figure 6**: Photocatalytic hydrogen generation of the fabricated photocatalyst under the different reaction conditions (a) under UV, (b) visible light irradiation, and (c) recycling stability experiments for photocatalytic $H_2$ performance under visible region after 4 cycles of $SrTiO_3$ and Ir doped $SrTiO_3$ photocatalyst.

energy gap of $SrTiO_3$. In general, these findings supply an insight into constructing a photocatalytic system by doping Ir into the semiconductor to coordinate the charge separation efficiency for clean energy production.

## COMPETING INTERESTS

The authors declare that there is no conflict of interest regarding the publication of this article.

## AUTHORS' CONTRIBUTIONS

Ton Nu Quynh Trang has conceived of the present idea, carried out and written the manuscript with support from Vu Thi Hanh Thu

Tieu Tu Doanh and Do Thanh Sinh has supported the analytical techniques

## ACKNOWLEDGMENTS

This research is funded by Vietnam National Foundation for Science and Technology Development (NAFOSTED) under grant number 103.99-2018.364.

## REFERENCES

1. Qin Q, Hao J, Zheng W. Ni/Ni3C core/shell hierarchical nanospheres with enhanced electrocatalytic activity for water oxidation. ACS applied materials & interfaces. 2018;10(21):17827–17834. PMID: 29726676. Available from: https://doi.org/10.1021/acsami.8b00716.
2. Zarrin S, Heshmatpour F. Photocatalytic activity of TiO2/Nb2O5/PANI and TiO2/Nb2O5/RGO as new nanocomposites for degradation of organic pollutants. Journal of hazardous materials. 2018;351:147–159. PMID: 29533887. Available from: https://doi.org/10.1016/j.jhazmat.2018.02.052.
3. Qin Q, Jang H, Chen L, Nam G, Liu X, Cho J. Low loading of RhxP and RuP on N, P codoped carbon as two trifunctional electrocatalysts for the oxygen and hydrogen electrode reactions. Advanced Energy Materials. 2018;8(29):1801478. Available from: https://doi.org/10.1002/aenm.201801478.
4. Trang TN, Phan TB, Nam ND, Thu VT. In situ charge transfer at the Ag@ZnO photoelectrochemical interface toward the high photocatalytic performance of H2 evolution and RhB degradation. ACS Applied Materials & Interfaces. 2020;12(10):12195–12206. PMID: 32013392. Available from: https://doi.org/10.1021/acsami.9b15578.
5. Trang TN, Tu LT, Man TV, Mathesh M, Nam ND, Thu VT. A high-efficiency photoelectrochemistry of Cu2O/TiO2 nanotubes based composite for hydrogen evolution under sunlight. Composites Part B: Engineering. 2019;174:106969. Available from: https://doi.org/10.1016/j.compositesb.2019.106969.
6. Odling G, Robertson N. Bridging the gap between laboratory and application in photocatalytic water purification. Catalysis Science & Technology. 2019;9(3):533–545. Available from: https://doi.org/10.1039/C8CY02438C.
7. Garg A, Singhania T, Singh A, Sharma S, Rani S, Neogy A, Yadav SR, Sangal VK, Garg N. Photocatalytic degradation of bisphenol-a using N, Co codoped TiO2 catalyst under solar light. Scientific reports. 2019;9(1):1–3. PMID: 30679732. Available from: https://doi.org/10.1038/s41598-018-38358-w.

8. Qian R, Zong H, Schneider J, Zhou G, Zhao T, Li Y, Yang J, Bahnemann DW, Pan JH. Charge carrier trapping, recombination and transfer during TiO2 photocatalysis: An overview. Catalysis Today. 2019;335:78–90. Available from: https://doi.org/10.1016/j.cattod.2018.10.053.
9. Amaniampong PN, Trinh QT, De Oliveira Vigier K, Dao DQ, Tran NH, Wang Y, Sherburne MP, Jérôme F. Synergistic Effect of High-Frequency Ultrasound with Cupric Oxide Catalyst Resulting in a Selectivity Switch in Glucose Oxidation under Argon. Journal of the American Chemical Society. 2019;141(37):14772–14779. PMID: 31450888. Available from: https://doi.org/10.1021/jacs.9b06824.
10. Tamiolakis I, Liu D, Xiao FX, Xie J, Papadas IT, Salim T, Liu B, Zhang Q, Choulis SA, Armatas GS. Mesoporous implantable Pt/SrTiO3: C, N nanocuboids delivering enhanced photocatalytic H2-production activity via plasmon-induced interfacial electron transfer. Applied Catalysis B: Environmental. 2018;236:338–347. Available from: https://doi.org/10.1016/j.apcatb.2018.05.036.
11. Wan S, Chen M, Ou M, Zhong Q. Plasmonic Ag nanoparticles decorated SrTiO3 nanocubes for enhanced photocatalytic CO2 reduction and H2 evolution under visible light irradiation. Journal of CO2 Utilization. 2019;33:357–364. Available from: https://doi.org/10.1016/j.jcou.2019.06.024.
12. Wrighton MS, Ellis AB, Wolczanski PT, Morse DL, Abrahamson HB, Ginley DS. Strontium titanate photoelectrodes. Efficient photoassisted electrolysis of water at zero applied potential. Journal of the American Chemical Society. 1976;98(10):2774–2779. Available from: https://doi.org/10.1021/ja00426a017.
13. Kiss B, Manning TD, Hesp D, Didier C, Taylor A, Pickup DM, Chadwick AV, Allison HE, Dhanak VR, Claridge JB, Darwent JR. Nano-structured rhodium doped SrTiO3-Visible light activated photocatalyst for water decontamination. Applied Catalysis B: Environmental. 2017;206:547–555. Available from: https://doi.org/10.1016/j.apcatb.2017.01.066.
14. Zhao G, Busser GW, Froese C, Hu B, Bonke SA, Schnegg A, et al. Anaerobic alcohol conversion to carbonyl compounds over nanoscaled Rh-Doped SrTiO3 under visible light. The journal of physical chemistry letters. 2019;10:2075–2080. PMID: 30973724. Available from: https://doi.org/10.1021/acs.jpclett.9b00621.
15. Amano F, Nakata M, Vequizo JJM, Yamakata A. Enhanced visible light response of TiO2 codoped with Cr and Ta Photocatalysts by electron doping. ACS Applied Energy Materials. 2019;2:3274–3282. Available from: https://doi.org/10.1021/acsaem.9b00126.
16. Munir S, Shah SM, Hussain H. Effect of carrier concentration on the optical bandgap of TiO2 nanoparticles. Materials & Design. 2016;92:64–72. Available from: https://doi.org/10.1016/j.matdes.2015.12.022.
17. Nazir S, Behtash M, Cheng J, Luo J, Yang K. Nb and Ta layer doping effects on the interfacial energetics and electronic properties of LaAlO3/SrTiO3 heterostructure: first-principles analysis. Physical Chemistry Chemical Physics. 2016;18(4):2379–2388. PMID: 26562134. Available from: https://doi.org/10.1039/C5CP05100B.
18. Wang G, Zhou M, Goettel JT, Schrobilgen GJ, Su J, Li J, Schlöder T, Riedel S. Identification of an iridium-containing compound with a formal oxidation state of IX. Nature. 2014;514(7523):475–477. PMID: 25341786. Available from: https://doi.org/10.1038/nature13795.
19. Kato H, Kudo A. Visible-light-response and photocatalytic activities of TiO2 and SrTiO3 photocatalysts codoped with antimony and chromium. The Journal of Physical Chemistry B. 2002;106(19):5029–5034. Available from: https://doi.org/10.1021/jp0255482.
20. Ma X, Cui X, Zhao Z, Melo MA, Roberts EJ, Osterloh FE. Use of surface photovoltage spectroscopy to probe energy levels and charge carrier dynamics in transition metal (Ni, Cu, Fe, Mn, Rh) doped SrTiO3 photocatalysts for H2 evolution from water. Journal of Materials Chemistry A. 2018;6(14):5774–5781. Available from: https://doi.org/10.1039/C7TA10934B.
21. Duong HP, Mashiyama T, Kobayashi M, Iwase A, Kudo A, Asakura Y, Yin S, Kakihana M, Kato H. Z-scheme water splitting by microspherical Rh-doped SrTiO3 photocatalysts prepared by a spray drying method. Applied Catalysis B: Environmental. 2019;252:222–229. Available from: https://doi.org/10.1016/j.apcatb.2019.04.009.
22. Menéndez-Flores VM, Ohno T. High visible-light active Ir-doped-TiO2 brookite photocatalyst synthesized by hydrothermal microwave-assisted process. Catalysis today. 2014;230:214–220. Available from: https://doi.org/10.1016/j.cattod.2014.01.032.
23. Kelly A, Knowles KM. Twinning. InCrystallography and Crystal Defects . John Wiley & Sons Ltd Chichester, UK . 2012;p. 335–361. Available from: https://doi.org/10.1002/9781119961468.ch11.
24. Luo J, Maggard PA. Hydrothermal synthesis and photocatalytic activities of SrTiO3-coated Fe2O3 and BiFeO3. Advanced Materials. 2006;18(4):514–517. Available from: https://doi.org/10.1002/adma.200500109.
25. Fadlallah MM, Shibl MF, Vlugt TJ, Schwingenschlögl U. Theoretical study on cation codoped SrTiO3 photocatalysts for water splitting. Journal of Materials Chemistry A. 2018;6(47):24342–24349. Available from: https://doi.org/10.1039/C8TA09022J.
26. Ma X, Cui X, Zhao Z, Melo MA, Roberts EJ, Osterloh FE. Use of surface photovoltage spectroscopy to probe energy levels and charge carrier dynamics in transition metal (Ni, Cu, Fe, Mn, Rh) doped SrTiO3 photocatalysts for H2 evolution from water. Journal of Materials Chemistry A. 2018;6(14):5774–5781. Available from: https://doi.org/10.1039/C7TA10934B.
27. Zhou X, Liu N, Yokosawa T, Osvet A, Miehlich ME, Meyer K, Spiecker E, Schmuki P. Intrinsically activated SrTiO3: photocatalytic H2 evolution from neutral aqueous methanol solution in the absence of any noble metal cocatalyst. ACS applied materials & interfaces. 2018;10(35):29532–29542. PMID: 30088904. Available from: https://doi.org/10.1021/acsami.8b08564.
28. Kiss B, Manning TD, Hesp D, Didier C, Taylor A, Pickup DM, Chadwick AV, Allison HE, Dhanak VR, Claridge JB, Darwent JR. Nano-structured rhodium doped SrTiO3-Visible light activated photocatalyst for water decontamination. Applied Catalysis B: Environmental. 2017;206:547–555. Available from: https://doi.org/10.1016/j.apcatb.2017.01.066.